Journal of Applied Physics ARTICLE scitation.org/journal/jap

Phase-dependent electronic and magnetic properties of Ti_2C monolayers

Cite as: J. Appl. Phys. **127**, 084302 (2020); doi: 10.1063/1.5140578
Submitted: 28 November 2019 · Accepted: 12 February 2020 ·
Published Online: 28 February 2020

B. Akgenc,[1] A. Mogulkoc,[2] and E. Durgun[3,a)]

AFFILIATIONS

[1]Department of Physics, Kirklareli University, Kirklareli 39100, Turkey
[2]Department of Physics, Faculty of Sciences, Ankara University, 06100 Tandogan, Ankara, Turkey
[3]UNAM—National Nanotechnology Research Center and Institute of Materials Science and Nanotechnology, Bilkent University, Ankara 06800, Turkey

[a)]**Author to whom correspondence should be addressed:** durgun@unam.bilkent.edu.tr

ABSTRACT

Achieving tunable magnetism in low-dimensions is an essential step to realize novel spintronic applications. In this manner, two-dimensional transition metal carbides/nitrides (MXenes) with intrinsic magnetism have attracted significant interest. In this study, we extensively examine the structural and magnetic properties of 1T- and 2H-Ti_2C monolayers by using first-principles techniques. We reveal the dynamical stability of both phases by using phonon spectra analysis and *ab initio* molecular dynamics simulations. The magnetic ground state is determined by considering all possible spin configurations and taking into account spin–orbit coupling effects, strong onsite Coulomb interaction, and corrected self-interaction terms. Our results indicate that while 1T-Ti_2C is anti-ferromagnetic, 2H-Ti_2C exhibits ferromagnetism, which is stable at/above room temperature. The electronic structure analysis demonstrates that 1T-Ti_2C is an indirect bandgap semiconductor and 2H-Ti_2C is a half-metal with 100% spin-polarization. Additionally, it is shown that the magnetic state is robust against low mechanical deformations and fundamental bandgap (also half-metallic bandgap) can be tuned by compressive/tensile strain. Phase-dependent and tunable electronic and magnetic properties of Ti_2C monolayers offer new opportunities in the field of low-dimensional magnetism.

I. INTRODUCTION

Two-dimensional (2D) transition metal carbides, nitrides, and carbonitrides (MXenes) are recent additions to the field of 2D materials,[1,2] and they have received significant attention following the synthesis of Ti_3C_2.[3] MXenes can be produced by extracting the A-group atomic layers from pristine phases that are identified with a general formula of $M_{n+1}AX_n$ (M: transition metal atom, A: Group XIII or XIV element, X: C and/or N).[4–6] Therefore, Ti_3C_2 actually belongs to a large family, many of which have been experimentally realized[2,7,8] or theoretically predicted.[1,9,10] MXenes possess unique properties depending on their constituent elements and/or surface terminations and they have been suggested as suitable materials for various applications such as alkali-ion batteries,[11,12] electrochemical capacitors,[13] thermoelectric systems,[14] optoelectronic devices,[15] water purification,[16] gas-sensors,[17] lubricants,[18] and topological insulators.[19]

Among the novel properties of MXenes, being intrinsically magnetic is of particular importance.[20] Most of the reported 2D systems are found as nonmagnetic (NM), thereof magnetic ordering (MO) can only be induced by external modifications (such as inclusion of adatoms[21] and/or defects[22]), which are experimentally challenging to realize and they also limit the potential usage. In this manner, several studies have focused on understanding the magnetic response of bare and functionalized derivatives of MXenes[23–29] to achieve tunable magnetism in low-dimensions, which is an undergoing challenge to be overcome.[6,7] Si *et al.* proposed that Cr_2C exhibits ferromagnetism with 100% spin-polarization due to itinerant *d*-electrons of Cr. Zhao *et al.* have studied the strain dependent electronic and magnetic properties of monolayer M2C (M = Hf, Ti, Nb, Sc, Ta, V, Zr) and concluded that while resulting magnetic moments are very sensitive to applied strain, the metallic characteristic is not altered even at high strain levels.[30] Gao *et al.* have investigated the stable monolayers of $Ti_2C(N)$, which have been found to be a ferromagnetic metal.[20]

Surface functionalization is also a critical factor that modifies fundamental properties of MXenes.[31–33] Champagne *et al.* have

investigated the electronic properties of bare and surface terminated V2C from first-principles calculations and they have showed that the metallic character of bare V2C is preserved for all surface groups.[34] Zhang *et al.* have demonstrated that the magnetic ground state of the Mn2C monolayer can be switched from antiferromagnetic (AFM) to ferromagnetic (FM) by full hydrogenation/oxygenation.[35] Urbankowski *et al.* have reported that while bare Ti4N3 is a FM metal with a high magnetic moment, surface terminations significantly modify its magnetic properties and -OH termination reduces the magnetic moment to almost zero, making it nonmagnetic.[8] In spite of the above-mentioned studies, the detailed investigation magnetic properties of MXenes are still scarce and phase dependence has not been considered yet.

With this motivation, we analyze the electronic and magnetic properties of the Ti2C monolayers that have been suggested for various applications[36,37] and their layered form has been recently realized in the 1T-phase.[7] Starting from geometry optimization, we first reveal the stability of bare 1T- and 2H-phases of Ti2C by considering phonon dispersion analysis and high temperature *ab initio* molecular dynamics (AIMD) calculations. Next, we examine the magnetic ground states by considering all possible spin orderings and taking into account spin–orbit coupling (SOC) effects, strong onsite Coulomb interaction, and corrected self-interaction terms. It is found that while the 1T-phase is an anti-ferromagnetic semiconductor, the 2H-phase is a ferromagnet exhibiting half-metallicity (i.e., being metallic for majority spin electrons and semiconductor for minority-spin electrons). The effect of low-strain on the electronic structure is studied, and the durability of the magnetic ground state under tensile/compressive strain is also demonstrated.

II. COMPUTATIONAL METHODOLOGY

The spin-polarized first-principles calculations were performed within the framework of density functional theory (DFT) implemented in the Vienna *ab initio* simulation package (VASP).[38,39] The projected augmented wave (PAW) potentials with a kinetic energy cutoff of 600 eV was used.[40] The exchange-correlation term was described with generalized-gradient approximation in Perdew–Burke–Ernzerhof formalism (GGA-PBE)[41] and hybrid functionals (HSE06).[42] The van der Waals (vdW) interaction was included by using the DFT-D2 method.[43] The strong onsite Coulomb interaction of localized *d*-orbitals was treated with DFT+U approach.[44] In this framework, the difference between the onsite Coulomb (U) and exchange (J) parameters was set to 2–5 eV in accordance with the reported values in the literature.[27,45] The spin–orbit coupling (SOC) effects were also taken into account. The Brillouin zone integration was performed by taking a Γ-centered $16 \times 16 \times 1$ *k*-point mesh for the unit cell. The lattice constants were optimized and atoms were relaxed without any constraint until the energy difference between two sequential steps was less than 10^{-5} eV, and maximum force on atoms was smaller than 10^{-3} eV Å^{-1}. The vacuum space of ∼20 Å was inserted along the *z*-direction to avoid the fictitious interactions generated due to periodic boundary conditions. The electronic charge transfers were calculated with decomposition of charge density into atomic contributions by applying the Bader charge analysis technique.[46]

The vibrational properties were obtained by the finite-displacement method implemented in the PHONOPY code.[47] *Ab initio* molecular dynamics (AIMD) simulations were carried out to examine the thermal stability of the Ti2C monolayers by using a $4 \times 4 \times 1$ super cell at 300 K, 600 K, and 900 K with the total simulation time of 3 ps and 2 fs time steps.

The cohesive energy (per unit cell) of 1T- and 2H-Ti_2C was calculated using the following relation:

$$E_C = 2 \times E_T(Ti) + E_T(C) - E_T(Ti_2C), \quad (1)$$

where $E_T(Ti)$ and $E_T(C)$ are the single isolated atom energies of Ti and C, and $E_T(Ti_2C)$ is the total energy of the 1T- or 2H-Ti_2C monolayer.

III. RESULTS AND DISCUSSION

Similar to 2D TMDs, monolayers of MXenes can also crystallize in the 1T- or 2H-phase.[35] Accordingly, in this study, both of the phases, unit cells of which are shown in Figs. 1(a) and 1(b), are taken into account. 1T- and 2H-Ti_2C structures represent P-3m1 and P-6m2 symmetries and are formed by sandwiching the C atomic layer between two Ti triangular sublattices where Ti atoms are arranged in a hexagonal geometry. In order to determine the magnetic ground states of both phases, a 2×2 super cell that contains eight Ti and four C atoms is constructed. We consider nonmagnetic (NM), ferromagnetic (FM), and antiferromagnetic (AFM) orderings. While there is only one possibility for NM and FM states, three coupling configurations exist for AFM (i.e., AFM1, AFM2, and AFM3, which are shown in Fig. S1 in the supplementary material). The comparison of total energies (E_T), which are obtained following structural optimizations including lattice constants for each magnetic states, implies that while the AFM2 ordering (where the spin of electrons of Ti atoms in the uppermost and lowermost atomic layers align in antiparallel arrangement) is preferred for 1T-Ti_2C, the lowest energy configuration is FM with $\mu = 2.0\mu_B$/cell for 2H-Ti_2C. It should be noted that previously the magnetic ground state of 1T-Ti_2C was reported as FM with $\mu = 1.91\mu_B$/cell[20] since not all of the AFM configurations were taken into account.

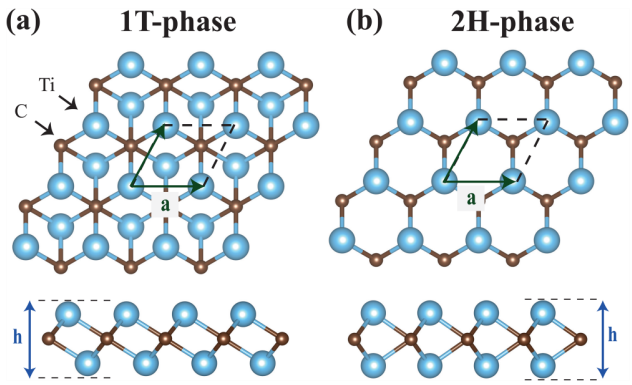

FIG. 1. Top and side views of (a) 1T- and (b) 2H-Ti_2C monolayers. Ti and C atoms are represented with blue and brown spheres, respectively.

TABLE I. The magnetic ordering (MO), the lattice constant (a), bonding distance between Ti and C (d_{Ti-C}), thickness (h), cohesive energy per unit cell (E_C), and total magnetic moment per unit cell (μ_B) for ground state configurations of 1T- and 2H-Ti_2C monolayers.

Phase	MO	a (Å)	d_{Ti-C} (Å)	h (Å)	E_C (eV)	$\mu(\mu_B)$
1T	AFM	3.07	2.11	2.29	19.27	0.00
2H	FM	3.05	2.15	2.47	18.04	2.00

However, E_T(AFM2) is 36 meV/cell lower than E_T(FM) (with $\mu = 1.89\mu_B$/cell) for 1T-Ti_2C.

The energy difference between spin-polarized and unpolarized state is significant for both phases and calculated as 105 meV/cell and 132 meV/cell for 1T- and 2H-Ti_2C, respectively, indicating the stability of magnetic configurations. In addition to the comparison of total energies, we also calculated the exchange interaction by using the Heisenberg model in which the Hamiltonian can be defined as

$$H = -\sum_{i,j} J_1(S_i \cdot S_j) - \sum_{k,l} J_2(S_k \cdot S_l), \quad (2)$$

where J_1 and J_2 are the first-nearest and the second-nearest exchange-coupling parameters. S is the net spin at the Ti sites, and (i, j) and (k, l) are the first-nearest and second-nearest site pairs, respectively. According to this model, exchange-coupling parameters are expressed as $J_1 = (E_T(AFM1) - E_T(FM))/12S^2$ and $J_2 = [(E_T(AFM2) - E_T(FM))/S^2 - 4J_1]/16$ and are calculated to be $J_1 = 6.80$ meV ($J_1 = -14.62$ meV) and $J_2 = 22.36$ meV ($J_2 = 22.84$ meV) for 2H-Ti_2C (1T-Ti_2C). Here, the minus sign demonstrates that the 1T-Ti_2C system prefers the antiferromagnetic ordering. The obtained values are comparable with the exchange-coupling parameters reported for Mn2C[35] and Cr2C[28] monolayers. Using the mean field approximation,[48] the Curie temperature of FM state can be calculated by using J parameters and estimated as ~290 K.

Following the determination of magnetic ordering, the structural properties are obtained for the ground state configurations and are summarized in Table I. The optimized lattice constants (a) of 1T- and 2H-Ti_2C are 3.07 Å and 3.05 Å with bonding distance between Ti and C (d_{Ti-C}) of 2.11 Å and 2.15 Å, respectively. The thickness (h) of the monolayer can be defined as the vertical distance between Ti sublattices and is equal to 2.29 Å and 2.47 Å for 1T- and 2H-Ti_2C, respectively. E_C of both phases is calculated by using Eq. (1) and it is found that $E_C(1T-Ti_2C)$ is 1.23 eV higher than $E_C(2H-Ti_2C)$. In a similar manner, the total energy (per unit cell) of the ground state configuration of 1T-Ti_2C is 1.23 eV higher than that of 2H-Ti_2C, which shows that the 1T-phase is energetically more favorable than the 2H-phase. The energy difference is within the same range of those that are reported for various transition metal dichlorides (TMDCs).[49]

Next, the dynamical stability of 1T- and 2H-Ti_2C monolayers is tested by calculating the corresponding phonon band structures. As illustrated in Figs. 2(a) and 2(b), all phonon modes of 1T- and

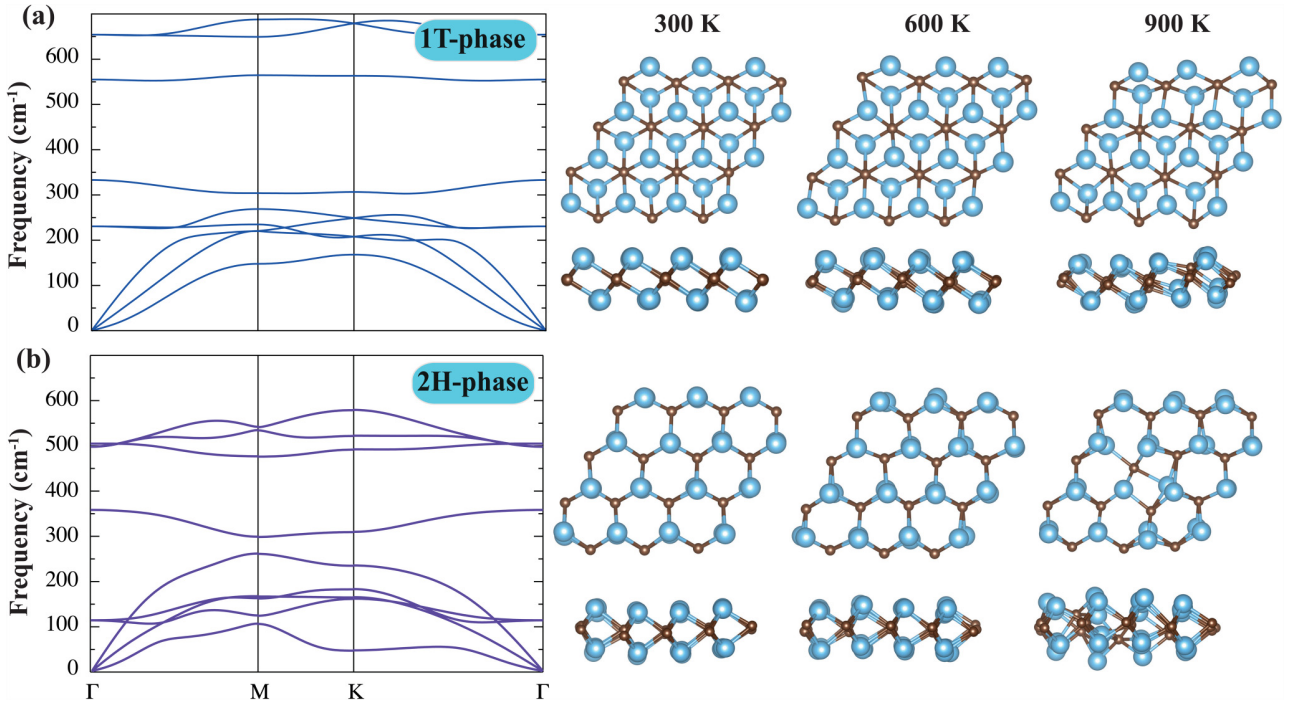

FIG. 2. The phonon band structures and snapshots of AIMD simulations (at 300 K, 600 K, and 900 K) for (a) 1T- and (b) 2H-Ti_2C monolayers.

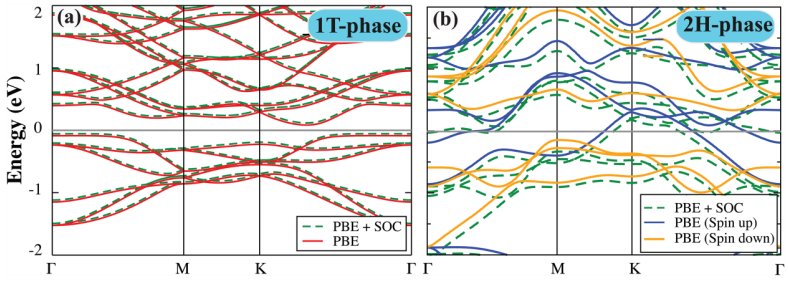

FIG. 3. The electronic band structures of (a) 1T- and (b) 2H-Ti_2C monolayers. Spin up and down bands are shown with solid blue and orange lines for 2H-Ti_2C, respectively. The bands including SOC are shown with dashed green lines. The Fermi level is set to zero and shown with gray line.

2H-Ti_2C have real eigenfrequencies indicating stable configurations. In addition to stability, the vibrational modes are analyzed at Γ-point. The decomposition is calculated as $\Gamma = 2E_g + 2E_u + A_{1g} + A_{2u}$ and $\Gamma = 2E'' + 2E' + A_1' + A_2''$ for 1T- and 2H-Ti_2C, respectively. The six optical phonon branches of 1T-Ti_2C consist of two non-degenerate out-of-plane modes (332 and 555 cm^{-1}) and two double-degenerate (230 and 654 cm^{-1}) in-plane vibrational modes. Similarly, the six optical phonon branches of 2H-Ti_2C also consist of two non-degenerate out-of-plane modes (355 and 502 cm^{-1}) and two double-degenerate (112 and 494 cm^{-1}) in-plane vibrational modes. Among the calculated modes, the E″, A_1', E_g, and A_{1g} modes are Raman active; A_2'', E_u, and A_{2u} modes are IR active; and the E′ mode is both Raman and IR active.

The thermal stability of 1T- and 2H-Ti_2C is further examined by *ab initio* molecular dynamics (AIMD) simulations [Figs. 2(a) and 2(b)]. Starting from 300 K, the temperature is stepwise increased to 600 K and then 900 K within 3 ps total simulation time. As can be noticed from the snapshots taken at the considered temperatures, apart from minor distortions, the crystallinity of both phases is preserved, implying the stability even at high temperatures. Additionally, magnetic moments calculated at 0 K are retained at 300 K, also indicating the stability of magnetic states at ambient temperature in agreement with the estimated Curie temperature (see above).

Following the confirmation of structural stability and revealing the magnetic ground states, the electronic band structures are examined. As shown in Fig. 3(a), 1T-Ti_2C is an AFM semiconductor with the calculated bandgap (E_{gap}^{PBE}) of 0.42 eV in its magnetic ground state. Its valence band minimum (VBM) and conduction band minimum (CBM) reside between K and Γ symmetry points, indicating the indirect bandgap character. Interestingly, the system is metallic for the FM (and also other AFM) configuration (Fig. S2 in the supplementary material). On the other hand, different from 1T-Ti_2C, 2H-Ti_2C exhibits half-metallicity where it is metallic for majority-spin electrons and semiconducting for minority-spin electrons. The half-metallic bandgap (i.e., bandgap for minority-spin electrons) is calculated as 0.54 eV. The dispersive metallic band arises mainly from itinerant Ti *d*-orbitals, clarifying why FM is energetically favored.[50] 2H-Ti_2C is metallic for all the other AFM configurations (Fig. S3 in the supplementary material). Due to valence *d*-electrons of Ti, the spin–orbit coupling (SOC) effects are expected to be significant. In that sense, SOC is included in electronic structure calculations (PBE+SOC) by setting the initial spin quantization axis as s_z. As can be noticed in Figs. 3(a) and 3(b), the

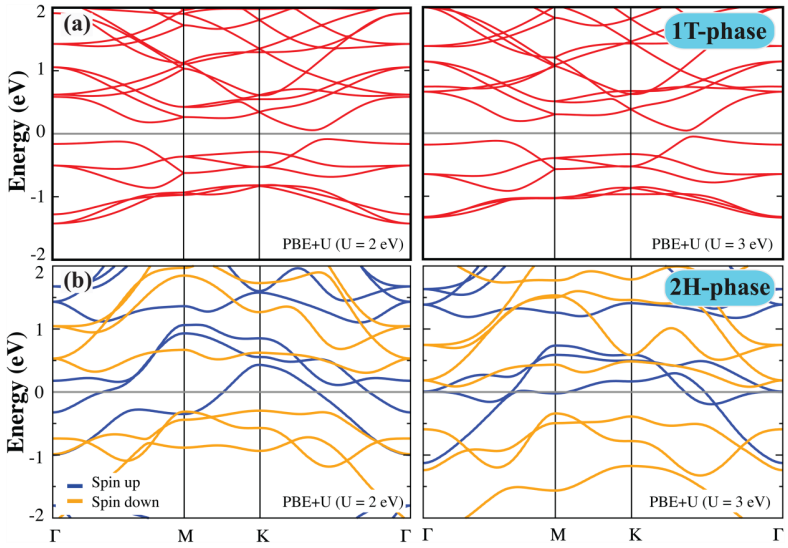

FIG. 4. The electronic band structures of (a) 1T- and (b) 2H-Ti_2C monolayers calculated at the level of PBE+U. Spin up and down bands are shown with solid blue and orange lines, respectively. The Fermi level is set to zero and shown with gray line.

SOC effect is minute in AFM 1T-Ti_2C; thus, the band profile is not altered and energy splitting is calculated as 31 meV. For 2H-Ti_2C, the SOC effect is more significant and it modifies dispersion of the bands, especially those arising from d-orbitals. The energy splitting is ~150 meV but the half-metallic (HM) character is preserved.

In order to properly calculate the strong onsite Coulomb interaction of *d*-electrons, the PBE+U approach is applied.[44] The strength of the interaction is described by U-J parameter (U and J correspond to Coulomb and exchange parameters, respectively), where J is fixed to 0 and U takes values between 2 and 5 eV based on earlier studies on 2D MXenes and TMDs.[20,23] The obtained electronic band structures with PBE+U (for U = 2 and U = 3) are shown in Figs. 4(a) and 4(b). With the inclusion of U, E_{gap}^{PBE+U} of 1T-Ti_2C decreases and the system even becomes semimetallic for higher values of U. A similar trend is also obtained when hybrid functionals (HSE and HSE+U) are used instead of GGA-PBE. For this case, as expected, E_{gap}^{HSE} is larger than E_{gap}^{PBE} and calculated as 0.48 eV due to the correction of the self-interaction error.[51,52] E_{gap}^{HSE} also decreases with increasing values of U (Fig. S4 in the supplementary material). For 2H-Ti_2C, however the HM character is preserved with the inclusion of U, the bandgap of minority-spin electrons (i.e., HM bandgap) decreases and also the dispersion of metallic majority-spin states are altered [Fig. 4(b)]. Similar to fundamental bandgap, implementing HSE also widens the HM bandgap (0.93 eV) (Fig. S4 in the supplementary material) and the minority-spin states remain to be semiconducting even for high U values confirming the HM character.

As strain engineering is a prominent strategy to tune the electronic properties of 2D materials,[53] lastly we examine the effect of low strain on the electronic structure of 1T- and 2H-Ti_2C monolayers at the level of GGA-PBE as shown in Figs. 5(a) and 5(b). We apply biaxial strain within the range of −3% to +3% ("−" and "+" sign indicate compressive and tensile strain, respectively) and reoptimize the atomic positions for each strain level. First, it should be noted that the transition from 1T- to 2H-phase (or vice versa) is not noticed even for higher strain values. For 1T-Ti_2C, E_{gap}^{PBE} decreases (Γ-K region) under compressive strain and becomes semi-metallic at −3% while preserving the AFM magnetic state. The applied tensile strain also decreases E_{gap}^{PBE} but the system remains to be semiconducting up to 3%. In addition to the alternation of the bandgap, the valence band dispersion (i.e., VBM) is drastically modified by tensile strain and becomes less dispersive, indicating a significant change in the effective mass of electrons. For 2H-Ti_2C, however the HM character of 2H-Ti_2C is preserved for tensile strain, HM bandgap decreases with compressive strain and 2H-Ti_2C transforms from HM to ferromagnetic metal at −2%. Similar results are obtained when uniaxial tensile/compressive strain is applied within low-strain levels.

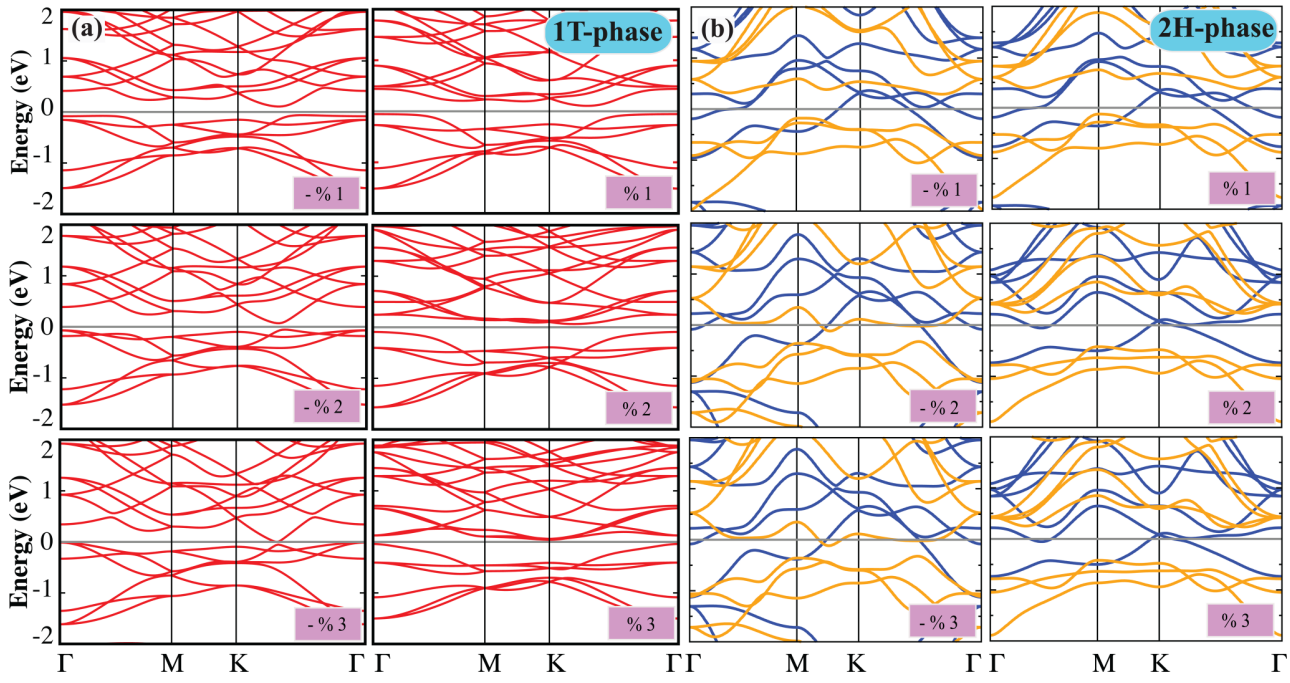

FIG. 5. The electronic band structures of (a) 1T- and (b) 2H-Ti_2C monolayers under compressive and tensile strain. Spin up and down bands are shown with solid blue and orange lines, respectively. The Fermi level is set to zero and shown with gray line.

IV. CONCLUSION

In summary, we investigate the structural, magnetic, and electronic properties of 1T- and 2H-Ti_2C monolayers. Phonon spectrum analysis and high temperature *ab initio* MD calculations reveal the dynamical stability of both phases. In order to determine the correct magnetic ground states, all possible spin configurations are tested and spin–orbit coupling effects (PBE-SOC), strong onsite Coulomb interaction (PBE+U), and corrected self-interaction terms (HSE06) are taken into account. Interestingly, while 1T-Ti_2C is found to be an anti-ferromagnetic semiconductor with an indirect bandgap, 2H-Ti_2C is a ferromagnetic half-metal with 100% spin-polarization. However, spin–orbit coupling effects are found to be significant, and it does not alter the magnetic ground state and the electronic structure of the monolayers. The *ab initio* MD calculations and the calculated Curie temperature confirm the stability of the magnetic ground state at ambient temperature. Finally, the effect of strain on the electronic band structure is examined and it is shown that the fundamental and half-metallic bandgap can be tuned by applying compressive/tensile strain, which can result in semiconductor (or half-metal) to metal transition. The intrinsic and stable magnetism of Ti_2C monolayers in addition to their phase-dependent electronic and magnetic properties point out these systems as promising materials, especially for low-power and miniaturized spintronic applications.

SUPPLEMENTARY MATERIAL

See the supplementary material for possible spin configurations, electronic band structures for AFM and FM magnetic states, and electronic band structures obtained with the HSE and HSE+U method, for 1T- and 2H-Ti_2C monolayers.

ACKNOWLEDGMENTS

This work was supported by the Scientific and Technological Research Council of Turkey (TUBITAK) under Project No. 117F383. The calculations were performed at the TUBITAK ULAKBIM, High Performance and Grid Computing Center (TR-Grid e-Infrastructure) and the National Center for High Performance Computing of Turkey (UHeM) under Grant No. 5003622015. A. Mogulkoc acknowledges the Ankara University for high performance computing facility through the AYP under Grant No. 17A0443001. B. Akgenc acknowledges financial support from the Kirklareli University-BAP under Project No. 189.

REFERENCES

[1]M. Naguib, V. N. Mochalin, M. W. Barsoum, and Y. Gogotsi, Adv. Mater. **26**, 992 (2014).
[2]K. Hantanasirisakul and Y. Gogotsi, Adv. Mater. **30**, 1804779 (2018).
[3]M. Naguib, M. Kurtoglu, V. Presser, J. Lu, J. Niu, M. Heon, L. Hultman, Y. Gogotsi, and M. W. Barsoum, Adv. Mater. **23**, 4248 (2011).
[4]J. L. Hart, K. Hantanasirisakul, A. C. Lang, B. Anasori, D. Pinto, Y. Pivak, J. T. van Omme, S. J. May, Y. Gogotsi, and M. L. Taheri, Nat. Commun. **10**, 522 (2019).
[5]M. Alhabeb, K. Maleski, B. Anasori, P. Lelyukh, L. Clark, S. Sin, and Y. Gogotsi, Chem. Mater. **29**, 7633 (2017).
[6]F. Shahzad, M. Alhabeb, C. B. Hatter, B. Anasori, S. M. Hong, C. M. Koo, and Y. Gogotsi, Science **353**, 1137 (2016).
[7]M. Naguib, O. Mashtalir, J. Carle, V. Presser, J. Lu, L. Hultman, Y. Gogotsi, and M. W. Barsoum, ACS Nano **6**, 1322 (2012).
[8]P. Urbankowski, B. Anasori, T. Makaryan, D. Er, S. Kota, P. L. Walsh, M. Zhao, V. B. Shenoy, M. W. Barsoum, and Y. Gogotsi, Nanoscale **8**, 11385 (2016).
[9]L. Wang, P. Hu, Y. Long, Z. Liu, and X. He, J. Mater. Chem. A **5**, 22855 (2017).
[10]B. Anasori, M. R. Lukatskaya, and Y. Gogotsi, Nat. Rev. Mater. **2**, 16098 (2017).
[11]Q. Tang, Z. Zhou, and P. Shen, J. Am. Chem. Soc. **134**, 16909 (2012).
[12]C. Eames and M. S. Islam, J. Am. Chem. Soc. **136**, 16270 (2014).
[13]Y. Dall'Agnese, P.-L. Taberna, Y. Gogotsi, and P. Simon, J. Phys. Chem. Lett. **6**, 2305 (2015).
[14]M. Khazaei, M. Arai, T. Sasaki, C.-Y. Chung, N. S. Venkataramanan, M. Estili, Y. Sakka, and Y. Kawazoe, Adv. Funct. Mater. **23**, 2185 (2013).
[15]K. Hantanasirisakul, M.-Q. Zhao, P. Urbankowski, J. Halim, B. Anasori, S. Kota, C. E. Ren, M. W. Barsoum, and Y. Gogotsi, Adv. Electron. **2**, 1600050 (2016).
[16]Q. Peng, J. Guo, Q. Zhang, J. Xiang, B. Liu, A. Zhou, R. Liu, and Y. Tian, J. Am. Chem. Soc. **136**, 4113 (2014).
[17]X.-F. Yu, Y.-C. Li, J.-B. Cheng, Z.-B. Liu, Q.-Z. Li, W.-Z. Li, X. Yang, and B. Xiao, ACS Appl. Mater. Interfaces **7**, 13707 (2015).
[18]X. Zhang, M. Xue, X. Yang, Z. Wang, G. Luo, Z. Huang, X. Sui, and C. Li, RSC Adv. **5**, 2762 (2015).
[19]H. Weng, A. Ranjbar, Y. Liang, Z. Song, M. Khazaei, S. Yunoki, M. Arai, Y. Kawazoe, Z. Fang, and X. Dai, Phys. Rev. B **92**, 075436 (2015).
[20]G. Gao, G. Ding, J. Li, K. Yao, M. Wu, and M. Qian, Nanoscale **8**, 8986 (2016).
[21]H. Sevinçli, M. Topsakal, E. Durgun, and S. Ciraci, Phys. Rev. B **77**, 195434 (2008).
[22]O. V. Yazyev, Rep. Prog. Phys. **73**, 056501 (2010).
[23]H. Kumar, N. C. Frey, L. Dong, B. Anasori, Y. Gogotsi, and V. B. Shenoy, ACS Nano **11**, 7648 (2017).
[24]G. Wang, J. Phys. Chem. C **120**, 18850 (2016).
[25]J. Hu, B. Xu, C. Ouyang, S. A. Yang, and Y. Yao, J. Phys. Chem. C **118**, 24274 (2014).
[26]N. C. Frey, A. Bandyopadhyay, H. Kumar, B. Anasori, Y. Gogotsi, and V. B. Shenoy, ACS Nano **13**, 2831 (2019).
[27]J. Zheng, R. He, Y. Wan, P. Zhao, P. Guo, and Z. Jiang, Phys. Chem. Chem. Phys. **21**, 3318 (2019).
[28]C. Si, J. Zhou, and Z. Sun, ACS Appl. Mater. Int. **7**, 17510 (2015).
[29]B. Akgenc, Comput. Mater. Sci. **171**, 109231 (2020).
[30]S. Zhao, W. Kang, and J. Xue, Appl. Phys. Lett. **104**, 133106 (2014).
[31]J.-J. Zhang and S. Dong, J. Chem. Phys. **146**, 034705 (2017).
[32]B. Akgenc, Turk. J. Phys. **43**, 531 (2019).
[33]B. Akgenc, Solid State Commun. **303**, 113739 (2019).
[34]A. Champagne, L. Shi, T. Ouisse, B. Hackens, and J.-C. Charlier, Phy. Rev. B **97**, 115439 (2018).
[35]X. Zhang, T. He, W. Meng, L. Jin, Y. Li, X. Dai, and G. Liu, J. Phys. Chem. C **123**, 16388 (2019).
[36]S. Zhao, W. Kang, and J. Xue, J. Phys. Chem. C. **118**, 14983 (2014).
[37]L.-Y. Gan, Y.-J. Zhao, D. Huang, and U. Schwingenschlögl, Phys. Rev. B **87**, 245307 (2013).
[38]G. Kresse and J. Hafner, Phys. Rev. B **47**, 558 (1993).
[39]G. Kresse and J. Furthmüller, Phys. Rev. B **54**, 11169 (1996).
[40]G. Kresse and D. Joubert, Phys. Rev. B **59**, 1758 (1999).
[41]J. P. Perdew, K. Burke, and M. Ernzerhof, Phys. Rev. Lett. **77**, 3865 (1996).
[42]J. Paier, M. Marsman, K. Hummer, G. Kresse, I. C. Gerber, and J. G. Ángyán, J. Chem. Phys. **124**, 154709 (2006).
[43]S. Grimme, J. Comput. Chem. **27**, 1787 (2006).
[44]S. Dudarev, G. Botton, S. Savrasov, C. Humphreys, and A. Sutton, Phys. Rev. B **57**, 1505 (1998).

[45]X. Chen, Z. Kong, N. Li, X. Zhao, and C. Sun, Phys. Chem. Chem. Phys. **18**, 32937 (2016).
[46]G. Henkelman, A. Arnaldsson, and H. Jónsson, Comput. Mater. Sci. **36**, 354 (2006).
[47]A. Togo and I. Tanaka, Scr. Mater. **108**, 1 (2015).
[48]C. Kittel *et al.*, *Introduction to Solid State Physics* (Wiley, New York, 1976), Vol. 8.
[49]Y. Feng, X. Wu, J. Han, and G. Gao, J. Mater. Chem. C **6**, 4087 (2018).
[50]H. Capellmann, Z. Phys. B **34**, 29 (1979).
[51]J. P. Perdew and M. Levy, Phys. Rev. Lett. **51**, 1884 (1983).
[52]P. Mori-Sánchez, A. J. Cohen, and W. Yang, Phys. Rev. Lett. **100**, 146401 (2008).
[53]Z. Dai, L. Liu, and Z. Zhang, Adv. Mater. **31**, 1805417 (2019).